Chin. J. Mech. Eng. (2017) 30:1305–1313
https://doi.org/10.1007/s10033-017-0186-1

ORIGINAL ARTICLE

Detection of Bearing Faults Using a Novel Adaptive Morphological Update Lifting Wavelet

Yi-Fan Li[1,2] · MingJian Zuo[1,3] · Ke Feng[1] · Yue-Jian Chen[3]

Received: 17 November 2016 / Revised: 27 July 2017 / Accepted: 29 September 2017 / Published online: 4 November 2017
© The Author(s) 2017. This article is an open access publication

Abstract The current morphological wavelet technologies utilize a fixed filter or a linear decomposition algorithm, which cannot cope with the sudden changes, such as impulses or edges in a signal effectively. This paper presents a novel signal processing scheme, adaptive morphological update lifting wavelet (AMULW), for rolling element bearing fault detection. In contrast with the widely used morphological wavelet, the filters in AMULW are no longer fixed. Instead, the AMULW adaptively uses a morphological dilation-erosion filter or an average filter as the update lifting filter to modify the approximation signal. Moreover, the nonlinear morphological filter is utilized to substitute the traditional linear filter in AMULW. The effectiveness of the proposed AMULW is evaluated using a simulated vibration signal and experimental vibration signals collected from a bearing test rig. Results show that the proposed method has a superior performance in extracting fault features of defective rolling element bearings.

Keywords Morphological filter · Lifting wavelet · Adaptive · Rolling element bearing · Fault detection

Supported by National Natural Science Foundation of China (51705431, 51375078) and Natural Sciences and Engineering Research Council of Canada (RGPIN-2015-04897).

✉ MingJian Zuo
ming.zuo@ualberta.ca

[1] School of Mechatronics Engineering, University of Electronic Science and Technology of China, Chengdu 611731, China

[2] School of Mechanical Engineering, Southwest Jiaotong University, Chengdu 610031, China

[3] Department of Mechanical Engineering, University of Alberta, Edmonton T6G 2G8, Canada

1 Introduction

Rolling element bearings, one of the most important and frequently used components in engineering machinery, play a critical role in system performances [1]. Effectively detecting the defects of rolling element bearings can provide an assurance for the reliability of machine sets.

When a localized fault occurs on the surface of the inner race, outer race or rolling element, the vibration signal would present repetitive peaks which are further modulated by rotational frequencies of machine components. The impulses contain important information about the bearing health status. Therefore, the extraction of cyclic faulty intervals is the essential task in bearing fault detection.

Many methods, such as wavelet transform [2], empirical mode decomposition [3], higher order spectrum [4], morphology filter [5] and order tracking [6] have been applied successfully in bearing fault detection and fault diagnosis. Wavelet transform (WT) is one of the most popular signal processing technologies among them. However, the classical WT, both continuous and discrete, are linear [7]. Because of the fact that a signal often contains information at many scales or resolutions, multi-resolution approaches are indispensable for a thorough understanding of such a signal. Therefore, it is desired to extend WT to nonlinear area.

The lifting scheme, proposed by Sweldens [8], has provided a useful way to design nonlinear wavelets. The flexibility and freedom offered by the lifting scheme have attracted researchers to develop various nonlinear WTs, including morphological ones. Not until 2000, Heijmans and Goutsias [9, 10] firstly gave the theoretical presentation of a general framework for constructing morphological wavelet (MW). The theoretical foundation of MW is extending the classic wavelet from the linear domain,

which is based on convolution, to the nonlinear domain, which is based on morphological operations. In this way, the MW does inherit the multi-dimension and multi-level analysis of wavelet while only involving the purely time domain analysis. As a consequence, a very high computational efficiency is achieved.

Following the work of Heijmans and Goutsias [9, 10], morphological gradient wavelet [11, 12], morphological undecimated wavelet (MUDW) [13–15] and morphological undecimated wavelet slices [16] were proposed and applied for fault detection and fault diagnosis. A major disadvantage of MW and the extended version is that the filter structure is fixed in the whole analysis process, which cannot cope with the sudden impulses and stationary data accurately in one signal at the same time. In many applications, it is desirable to have a filterbank that somehow determines how to shape itself according to the signal being analyzed. Based on this consideration, Piella and Heijmans [17] proposed an adaptive update lifting wavelet (AULW). The basic idea underlying AULW is to employ different update lifting filters to modify the approximation signal according to the signal local gradient information. However, the essence of AULW is still linear wavelet decomposition. The effectiveness of employing AULW to process the real mechanical vibration signals is actually compromised.

A new method of morphological lifting scheme, an adaptive morphological update lifting wavelet (AMULW) is proposed in this study. The aim of AMULW is to address the disadvantages both from the linear wavelet decomposition and from the fixed filter in AULW and MW. In AMULW, the nonlinear morphological dilation-erosion filter, as well as the average filter, is adaptively adopted in the update lifting scheme according to the geometry of the signal. Consequently, the impulsive features would be strengthened and the noise would be suppressed effectively.

The rest of this paper is organized as follows: Section 2 briefly introduces the fundamentals of MW; Section 3 proposes the AMULW; the advantage of AMULW over the AULW and MUDW is demonstrated by using a simulated vibration signal in Section 4; Section 5 applies the proposed AMULW technique to experimental signals of rolling element bearings and demonstrates the detection ability of AMULW for an inner race fault bearing and an outer race fault bearing; Conclusions are drawn in Section 6.

2 Morphological Wavelet

Figure 1 illustrates a one stage uncoupled MW decomposition scheme [10].

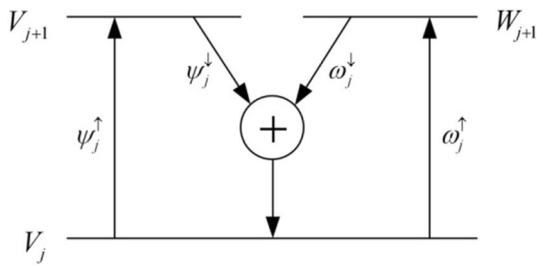

Figure 1 Schematics of MW

Consider a family V_j, V_{j+1} and W_{j+1} of signal spaces. There are two analysis operators $\psi_j^{\uparrow}$ and $\omega_j^{\uparrow}$ which together decompose a signal in the direction of increasing j. The signal analysis operator $\psi_j^{\uparrow}$ maps a signal from V_j to V_{j+1} and the detail analysis operator $\omega_j^{\uparrow}$ maps a signal from V_j to W_{j+1}.

$$\begin{aligned} &\psi_j^{\uparrow}(\psi_j^{\downarrow}(x)+\omega_j^{\downarrow}(y))=x \qquad x\in V_{j+1}, y\in W_{j+1} \\ &\omega_j^{\uparrow}(\psi_j^{\downarrow}(x)+\omega_j^{\downarrow}(y))=y \qquad x\in V_{j+1}, y\in W_{j+1} \end{aligned} \tag{1}$$

where x is the approximation signal and y is the detail signal. The signal and detail analysis operators correspond to a low pass and a high pass filter, respectively [10].

On the other hand, a synthesis operator + proceeds in the direction of decreasing j. For the purpose of yielding a complete signal representation, the analysis mapping $(\psi_j^{\uparrow}, \omega_j^{\uparrow})$: $V_j \to V_{j+1} \times W_{j+1}$ and synthesis mapping $(\psi_j^{\downarrow} + \omega_j^{\downarrow})$: $V_{j+1} \times W_{j+1} \to V_j$ should be inverse of each other, which means the following condition should be satisfied:

$$\psi_j^{\downarrow}\psi_j^{\uparrow}(x)+\omega_j^{\downarrow}\omega_j^{\uparrow}(x)=x \qquad x\in V_j \tag{2}$$

This condition is called the perfect reconstruction [17]. A raw signal x_0 can be decomposed with the following recursive analysis scheme:

$$\begin{aligned} x_0 &\to \{x_1, y_1\} \to \{x_2, y_2, y_1\} \to \cdots \\ &\to \{x_n, y_n, y_{n-1}, y_{n-2}, \cdots, y_2, y_1\} \end{aligned} \tag{3}$$

And x_0 also can be exactly reconstructed from x_n, y_n, y_{n-1}, y_{n-2}, …, y_2, y_1 through the recursive synthesis scheme shown in Eq. (4).

$$\begin{aligned} &x_j=\psi_j^{\downarrow}(x_{j+1})+\omega_j^{\downarrow}(y_{j+1}) \\ &j=n-1, n-2, \cdots, 0 \end{aligned} \tag{4}$$

In MW, the analysis operator $\psi_j^{\uparrow}$ and the synthesis operator $\psi_j^{\downarrow}$ are morphological operators. Some MWs have been established, such as morphological Haar wavelet [18].

3 Adaptive Morphological Update Lifting Wavelet

3.1 Principles of AMULW

The schematic of the proposed AMULW in one stage is illustrated in Figure 2. In AMULW, the update lifting is applied to modify the approximation signal, while the detail signal remains unchanged in the decomposition process, namely $y_1' = y_1$.

The AMULW comprises three main steps. First, the raw signal x_0 is split into two parts, producing an approximation signal x_1 and a detail signal y_1. This partition can be fulfilled by some special wavelet transform. The simplest one is to directly split x_0 into odd and even samples [19]:

$$\begin{aligned} x_1 &= \psi^{\uparrow}(x_0)(n) = x_0(2n) \\ y_1 &= \omega^{\uparrow}(x_0)(n) = x_0(2n+1) \end{aligned} \tag{5}$$

Then, a two-valued decision map D is used to control the choice of the update filter, which is expressed as follows:

$$D(n) = \begin{cases} 1 & g(n) > T \\ 0 & g(n) \le T \end{cases} \tag{6}$$

where T is the threshold value; $g(n)$ denotes the local gradient information of adjacent three samples in a signal, which is defined as:

$$g(n) = |x_1(n) - y_1(n-1)| + |y_1(n) - x_1(n)| \tag{7}$$

Subsequently, the approximation signal x_1 is updated using the information hidden in the detail signal y_1, yielding a new approximation signal x_1'. If $D(n) = 1$, the morphological dilation-erosion filter is used as the update operator U_1:

$$U_1(n) = y_1(n-1) \wedge y_1(n) - y_1(n-1) \vee y_1(n) \tag{8}$$

$$\begin{aligned} x_1'(n) &= x_1(n) + U_1(n) = x_1(n) + \\ & y_1(n-1) \wedge y_1(n) - y_1(n-1) \vee y_1(n) \end{aligned} \tag{9}$$

where $\vee$ represents morphological dilation operation and $\wedge$ represents morphological erosion operation.

If $D(n) = 0$, the average filter is utilized as the update operator U_0:

$$U_0(n) = y_1(n-1) + y_1(n) \tag{10}$$

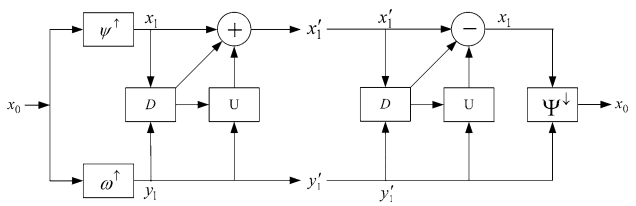

Figure 2 Schematic of AMULW

$$\begin{aligned} x_1'(n) &= \frac{1}{3}(x_1(n) + U_0(n)) \\ &= \frac{1}{3}(x_1(n) + y_1(n-1) + y_1(n)) \end{aligned} \tag{11}$$

Correspondingly, x_1 can be easily reconstructed from x_1' and y_1' as Eq. (12) or (13). Once x_1 is obtained, the synthesis signal x_0 is also easy to get.

$$x_1(n) = x_1'(n) + y_1(n-1) \vee y_1(n) - y_1(n-1) \wedge y_1(n) \tag{12}$$

$$x_1(n) = 3x_1'(n) - y_1(n-1) - y_1(n) \tag{13}$$

The above analysis process is limited to the scope of one stage decomposition. A raw signal x_0 can be decomposed into multiple levels as a multiple stage decomposition involves:

$$\begin{aligned} x_0 \to \{x_1', y_1'\} \to \{x_2', y_2', y_1'\} \to \cdots \\ \to \{x_n', y_n', y_{n-1}', y_{n-2}', \cdots, y_2', y_1'\} \end{aligned} \tag{14}$$

On account of the presence of the decision map D, the update lifting operator U can be adaptively selected to modify the approximation signal. The morphological dilation-erosion filter is adopted to strengthen the impulsive features when there is an impulse in a signal, while the average filter is employed to smooth a signal at the time when the signal amplitudes vary weakly.

3.2 The Selection of the Threshold T

The function of the threshold T is to distinguish the stationary data and the impulses in a signal. If T is too large, some useful impulsive information might be smoothed by using the average filter; on the contrary, if T is too small, some tiny fluctuations might be treated as impulses. In the present paper, T is defined as:

$$T = k \cdot \max(g(n)) \qquad k \in [0, 1] \tag{15}$$

In order to reduce the adverse effects of the threshold T, we perform the AMULW multiple times with k increasing from 0 to 1, with a step size of 0.1. As a result, 11 analysis results would be obtained. Then, characteristic frequency intensity coefficient (CFIC) [20] of the above 11 signals are computed. The CFIC can be expressed as:

$$\mathrm{CFIC} = \frac{\sum_{i=1}^{N} A_{if_c}}{\sum_{j=1}^{M} A_{f_j}} \tag{16}$$

where A_{if_c} is the amplitude of the ith harmonic of the fault characteristic frequency, N is the number of the harmonics of the fault characteristic frequency, A_{f_j} is the amplitude of

the frequencies analyzed, and M is the number of all frequency components.

The CFIC represents the portion of the fault frequency amplitude to the overall frequency amplitude. A larger value of CFIC implies a better fault detection performance. Other statistic criterion, such as kurtosis [21], smoothness index [22], crest factor [23], peak energy [24] and fusion criterion of kurtosis, smoothness index and crest factor [25], can also be used as a guide to select the fault relevant information. In this study, CFIC is employed. The signal with the largest CFIC value is picked out from the whole 11 candidates and only this signal will be utilized in the fault detection.

3.3 Perfect Reconstruction

Assume that α, β and γ are lifting wavelet coefficients:

$$x_1'(n) = \alpha x_1(n) + \beta y_1(n-1) + \gamma y_1(n) \tag{17}$$

Ref. [17] has proved in theory that in order to fulfill perfect reconstruction, it requires:

$$\alpha + \beta + \gamma = M \tag{18}$$

where M is a constant and usually set as 1.

In Eq. (11), $\alpha = \beta = \gamma = 1/3$, which meets the requirement of Eq. (18). For Eq. (9), we discuss the influence of the value of $y_1(n-1)$ and $y_1(n)$ on perfect reconstruction. In summary, there are three situations:

Case 1: $y_1(n-1) > y_1(n)$, at this moment Eq. (9) can be simplified as

$$x_1'(n) = x_1(n) + y_1(n) - y_1(n-1) \tag{19}$$

Case 2: $y_1(n-1) < y_1(n)$, at this moment Eq. (9) can be simplified as

$$x_1'(n) = x_1(n) + y_1(n-1) - y_1(n) \tag{20}$$

Case 3: $y_1(n-1) = y_1(n)$, at this moment Eq. (9) can be simplified as

$$x_1'(n) = x_1(n) \tag{21}$$

Regardless the value of $y_1(n-1)$ and $y_1(n)$, the situations in Eqs. (19)–(21) accords with the requirement of Eq. (18). Therefore, the proposed AMULW fits the perfect reconstruction condition.

4 Simulated Signal Analysis

A vibration signal $s(t)$ of rolling element bearing under an inner race fault condition is simulated [26] to evaluate the effective of the proposed AMULW. The sampling frequency f_s of signal $s(t)$ is 4096 Hz and the samples are 4096. The signal $s(t)$ is made up of three parts:

$$s(t) = s_1(t) + s_2(t) + s_3(t) \tag{22}$$

where $s_1(t)$ is the periodic impulse response model of a defective bearing [21]:

$$s_1(t) = \sum_i A_i u(t - iT - \tau_i) + n(t) \tag{23}$$

where i is the number of impulses; A_i is the amplitude modulator; T stands for the fault impacts repetitive period, which gives the reciprocal of fault characteristic frequency f_c; τ_i represents the minor and random time fluctuation around T; $n(t)$ denotes the stationary noise; and $u(\cdot)$ is fault impulse function:

$$u(t) = e^{-at}\sin(2\pi f_0 t + \varphi) \tag{24}$$

where a is the decay parameter, f_0 the fault excited resonance frequency and φ the original phase.

For an inner race fault, A_i in Eq. (23) can be simplified as [27]

$$A_i = A_0 + A_0'\cos(2\pi f_A(iT + \tau_i) + \varphi_A) \tag{25}$$

where A_0 and A_0' are the mean and maximum of the amplitude modulator, respectively; f_A equals to the shaft frequency; $iT + \tau_i$ denotes the special time point at the ith impulse; and φ_A is related to the location of the sensor.

The parameters for the simulation of vibration signal $s_1(t)$ are shown in Table 1.

In Eq. (22), $S_2(t) = 0.2\sin(2\pi 10t) + 0.4\cos(2\pi 25t)$ simulates two interference frequencies, $s_3(t)$ represents a Gaussian white noise. The signal-to-noise ratio of $s(t)$ is 0 dB.

Figure 3 presents the simulated signal $s(t)$ and its corresponding fast Fourier transform (FFT) spectrum. As it can be seen that the fault related characteristic frequency 16 Hz along with its harmonics are totally overwhelmed by the interference signals (10 and 25 Hz) and the noise.

The approximation signal obtained by AMULW is presented in Figure 4(a). This approximation signal obtained by AMULW is at level 3 of the decomposition process. Wavelet decomposition algorithm is the down-sampling procedure that the length of approximation signal and detail signal would halve as the decomposition level increasing. Suppose that the length of raw signal is L, the data number of approximation signal and detail signal

Table 1 Parameters used in the simulation of signal $s_1(t)$

i	A	T	τ_i	$n(t)$
16	[3, 4]	1/16	0	0
a	f_0	ϕ	ϕ_A	
100	600	0	0	

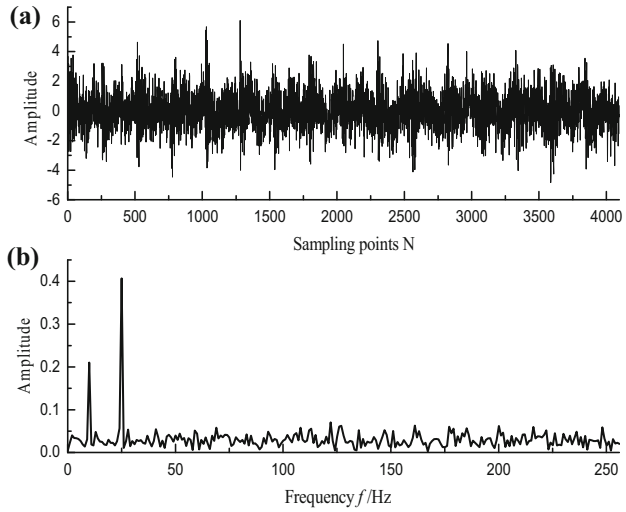

Figure 3 Simulated signal: (a) time-domain waveform, (b) frequency spectrum

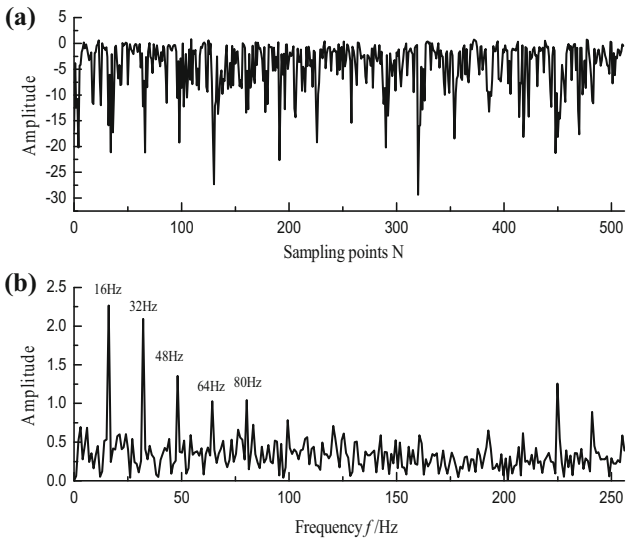

Figure 4 AMULW analysis results of the simulated signal: (a) time-domain waveform, (b) frequency spectrum

would be $L/2^n$ after n decompositions. Therefore, only 512 samples are shown in Figure 4(a). The parameter k is set at 0.2 because at this time the analysis result has the maximum CFIC value. As shown in Figure 4(b), the impulsive characteristic frequency of 16, 32, 48, 64 and 80 Hz are identified clearly and the interferences of 10 and 25 Hz are totally restrained.

The simulated signal shown in Figure 3(a) is analyzed by AULW [17]. Figure 5 displays the analysis results in the time domain and its FFT spectrum. Although some impulsive characteristic frequencies are detected, 10 Hz and 25 Hz as well as other interferences are still present. Comparing with Figure 4(b), the AULW is less effective

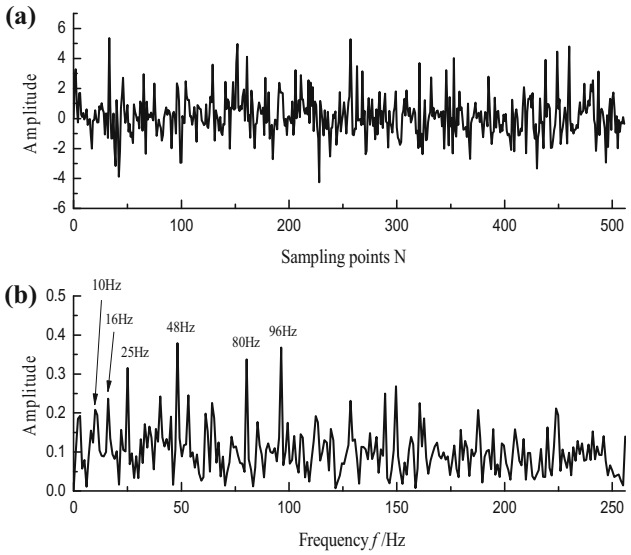

Figure 5 AULW analysis results of the simulated signal: (a) time-domain waveform, (b) frequency spectrum

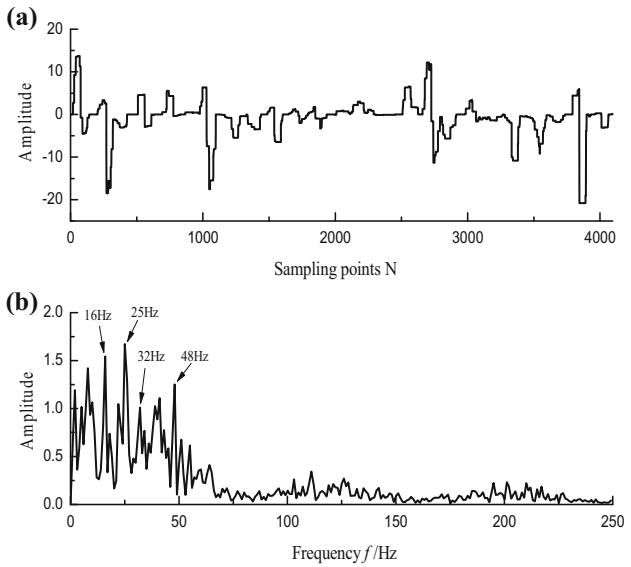

Figure 6 MUDW analysis results of the simulated signal: (a) time-domain waveform, (b) frequency spectrum

than the proposed method to extract impulsive features and restrain interferences.

The MUDW [14] procedure is applied to the simulated signal with three levels of decomposition. The approximation signal at level 3 and its frequency spectrum are shown in Figure 6. MUDW is a non-decimation decomposition method and it omits down-sampling in the forward transform. Therefore, the approximation signal and the detail signal are of the same length as the raw signal whatever level they are at. Unfortunately, the spectral line 25 Hz in Figure 6(b) is visually obvious, which comes

from the interference signal $s_2(t)$. Hence, in this case, AMULW is more effective in extracting the features.

5 Experimented Lab Signal Analysis

In this section, the performance of the proposed AMULW is graphically evaluated by using vibration signals of rolling element bearings. The experiment was conducted at Engineering Reliability, Prognostic and Health Management Laboratory, University of Electronic Science and Technology of China. The experimental set-up consists of a shaft, two bearings and a bevel gearbox. It is driven by a 2.24 kW three phase electrical motor controlled by a motor speed controller. The bearing system is under consideration for fault diagnosis. An accelerometer (with sensitivity of 100 mV/g and frequency range 0–10 kHz) and a shaft encoder are used for capturing the vibration signals and rotating speed signals simultaneously. The whole set-up arrangement is displayed in Figure 7.

5.1 Analysis of the Vibration Signal of Bearing with an Inner Race Fault

For the rotor with a rotating speed at 1800 r/min, vibration signal of the defective bearing with an inner race fault and its FFT spectrum are illustrated in Figure 8, sampled at a frequency of 20480 Hz. The theoretical rotational frequency f_r of the shaft is 30 Hz and ball pass frequency in inner race (BPFI) is 163 Hz. But the BPFI cannot be identified in Figure 8(b).

The AMULW method is applied to the rolling element bearing vibration signal presented in Figure 8(a). Figure 9(a) shows the approximation signal at the third level of AMULW decomposition. The parameter k is determined as 0.2 according to multiple trials as well. Figure 9(b) plots the frequency spectrum where the defective feature frequencies of the bearing can be identified. The BPFI together with its second-order and third-order harmonics, 2BPFI and 3BPFI, side frequencies BPFI $- 2f_r$, BPFI $+ 2f_r$, 2BPFI $- 2f_r$, 2BPFI $+ 2f_r$, 3BPFI $- 2f_r$, and the second harmonic of modulation frequency $2f_r$ are all detected. These frequency components clearly indicate an inner race fault on the bearing.

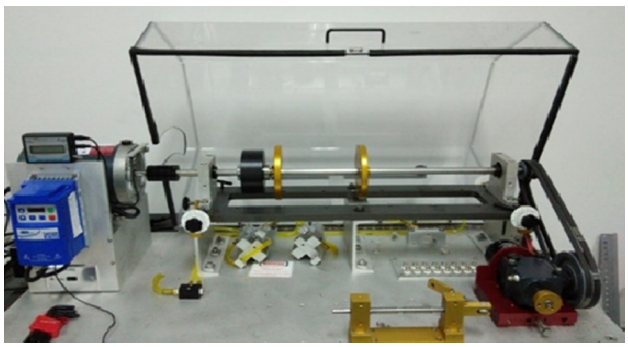

Figure 7 Experimental setup

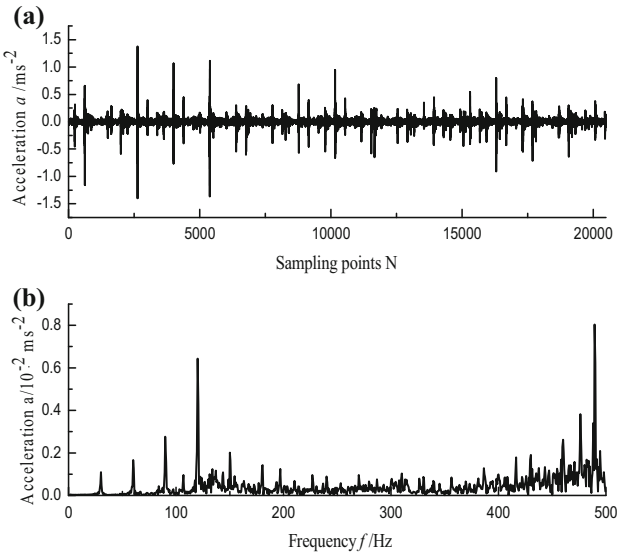

Figure 8 Vibration signal of inner race fault bearing: (a) time-domain waveform, (b) frequency spectrum

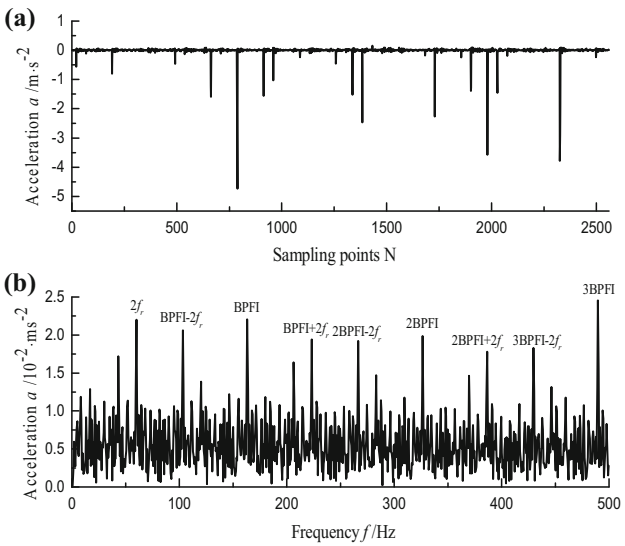

Figure 9 Vibration signal of inner race fault bearing after AMULW analysis: (a) time-domain waveform, (b) FFT spectrum

In Figure 10, the analysis results of AULW are presented, from which it can be found that the $4f_r$ and 3BPFI could be clearly detected in the Fourier spectrum, while the BPFI and its side frequencies are not particularly evident. Therefore, the accuracy of using AULW to diagnose this inner race fault bearing is actually poor.

Figure 11 demonstrates the analysis results of MUDW. In Figure 11(b), some characteristic frequencies are

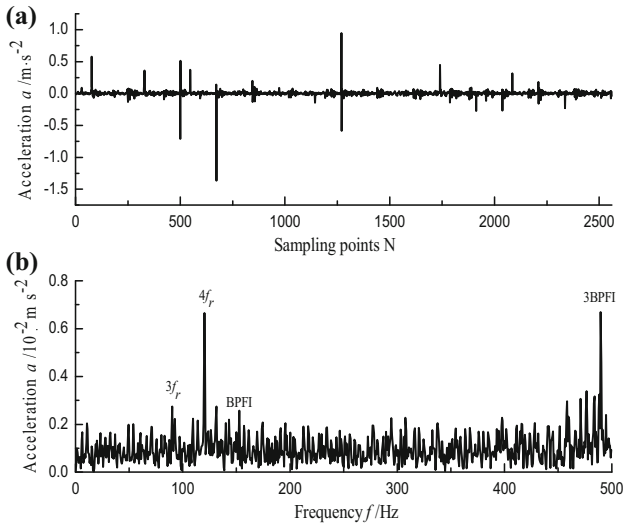

Figure 10 Vibration signal of inner race fault bearing after AULW analysis: (a) time-domain waveform, (b) FFT spectrum

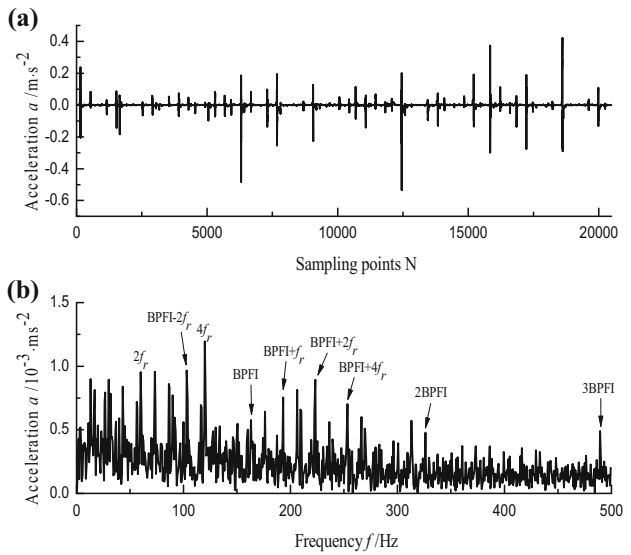

Figure 11 Vibration signal of inner race fault bearing after MUDW analysis: (a) time-domain waveform, (b) FFT spectrum

detected, such as BPFI, 2BPFI, 3BPFI, BPFI + $2f_r$, BPFI − $2f_r$, etc. These frequency components indicate an inner race fault on the bearing. The effectiveness of employing MUDW to detect this bearing fault is much better than AULW. However, these fault related features shown in Figure 11(b) is not as apparent as Figure 9(b).

5.2 Analysis of the Vibration Signal of Bearing with Outer Race Fault

The vibration signal of a bearing with a fault in outer race was collected at the sampling frequency of 20480 Hz. The shaft rotation frequency f_r and ball pass

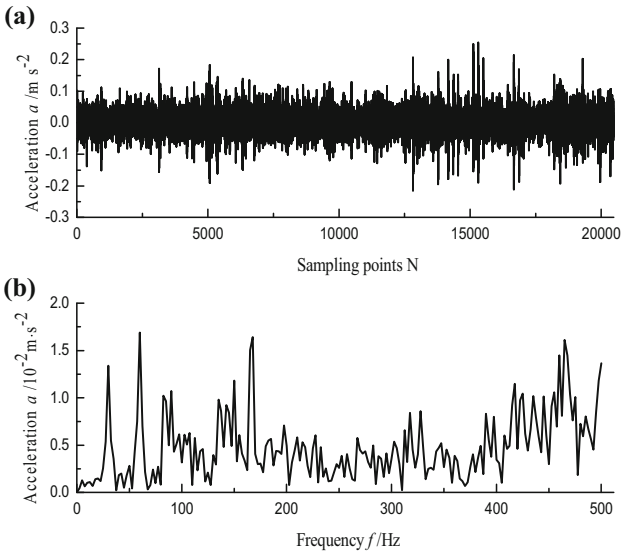

Figure 12 Vibration signal of outer race fault bearing: (a) time-domain waveform, (b) frequency spectrum

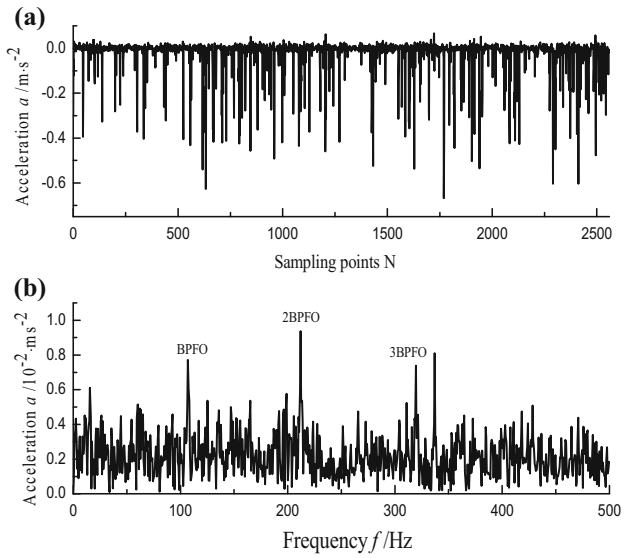

Figure 13 Vibration signal of outer race fault bearing after AMULW analysis: (a) time-domain waveform, (b) FFT spectrum

frequency in outer race (BPFO) are 30 Hz and 107 Hz, respectively. Figure 12 shows the time waveform and the FFT spectrum of this signal. The fault frequency BPFO cannot be determined, as shown in the FFT spectrum of Figure 12(b).

The AMULW analysis results are shown in Figure 13. The approximation signal at the third level of AMULW decomposition and its FFT spectrum, are presented in Figure 13(a) and (b) respectively. The parameter k is selected at 0.2. The BPFO and its second harmonic 2BPFO and third harmonic 3BPFO can be clearly identified in Figure 13(b). There is a good match between the estimated

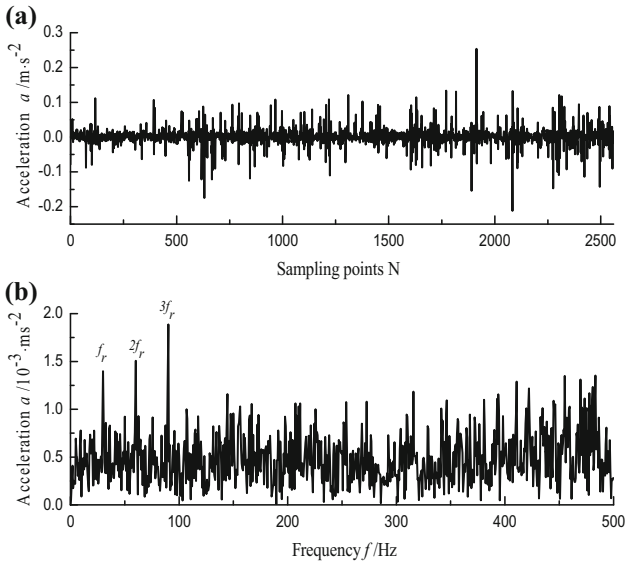

Figure 14 Vibration signal of outer race fault bearing after AULW analysis: (a) time-domain waveform, (b) FFT spectrum

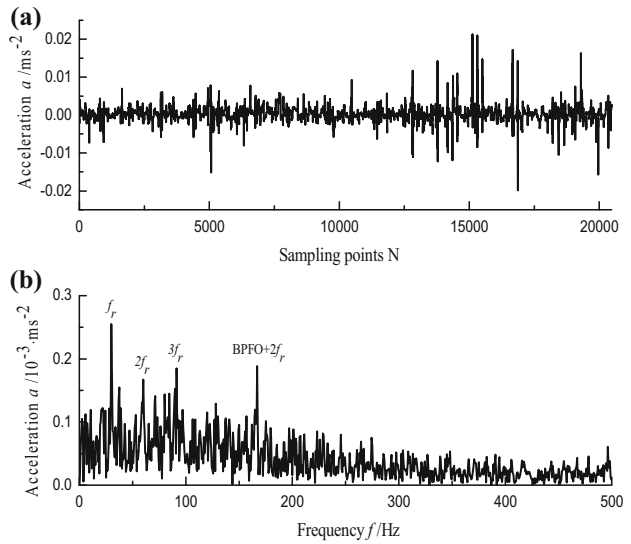

Figure 15 Vibration signal of outer race fault bearing after MUDW analysis: (a) time-domain waveform, (b) FFT spectrum

features and the actual fault features associated with the rolling element bearing with the outer race defect.

Figures 14 and 15 describe the analysis results of AULW and MUDW, respectively. The frequency spectrum in Figures 14(b) and 15(b) are not suitable for indicating a bearing with an outer race fault. Therefore, both of the two methods fail to identify this fault. The ability of AULW and MUDW for detecting the rolling element bearing with outer race fault is inferior to AMULW.

6 Conclusions

In this paper, an AMULW with perfect reconstruction is developed to detect rolling element bearing faults. Compared with Fourier transforms using the same filter and wavelets being translation and dilation of one given function, lifting scheme adapts local data irregularities in the transform process. In the proposed AMULW, two filters are adaptively employed. The nonlinear morphological dilation-erosion filter is effective to extract impulses while the average filter is suitable for removing noise. Therefore, AMULW can reasonably process a non-stationary mechanical vibration signal comprising of impulses and interferences. The experimental evaluation results have shown that the proposed AMULW is capable of extracting the impulsive features of the bearing vibration signals. It outperforms AULW in detection both of an inner race fault and an outer race fault of a rolling element bearing and it outperforms MUDW in detection of an outer race fault of a rolling element bearing.

Open Access This article is distributed under the terms of the Creative Commons Attribution 4.0 International License (http://creativecommons.org/licenses/by/4.0/), which permits unrestricted use, distribution, and reproduction in any medium, provided you give appropriate credit to the original author(s) and the source, provide a link to the Creative Commons license, and indicate if changes were made.

References

1. R B Randall, J Antoni. Rolling element bearing diagnostics – a tutorial. *Mechanical Systems and Signal Processing*, 2001, 25: 945–962.
2. R Q Yan, R Gao, X F Chen. Wavelets for fault diagnosis of rotary machines: A review with application. *Signal Processing*, 2014, 96: 1–15.
3. Y G Lei, J Lin, Z J He, et al. A review on empirical mode decomposition in fault diagnosis of rotating machinery. *Mechanical Systems and Signal Processing*, 2013, 35(1): 108–126.
4. Z P Feng, M Liang, F L Chu. Recent advances in time-frequency analysis methods for machinery fault diagnosis: A review with application examples. *Mechanical Systems and Signal Processing*, 2013, 38: 165–205.
5. Y F Li, X H Liang, M J Zuo. A new strategy of using a time-varying structure element for mathematical morphological filtering. *Measurement*, 2017, 106: 53–65.
6. K Feng, K S Wang, M Zhang, et al. A diagnostic signal selection scheme for planetary gearbox vibration monitoring under non-stationary operational conditions, *Measurement Science and Technology*, 2017, 28(3): 035003 (10 pp).
7. H Heijmans, B Pesquet-Popescu, G Piella. Building nonredundant adaptive wavelets by update lifting. *Applied and Computational Harmonic Analysis*, 2005, 18: 252–281.
8. W Sweldens. The lifting scheme: A construction of second generation wavelets. *Siam Journal on Mathematical Analysis*, 1998, 29(2): 511–546.

9. J Goutsias, H Heijmans. Nonlinear multiresolution signal decomposition schemes—Part 1: Morphological pyramids. *IEEE Transactions on Image Processing*, 2000, 9(11): 1862–1876.
10. H Heijmans, J Goutsias. Nonlinear multiresolution signal decomposition schemes—Part 2: Morphological wavelets. *IEEE Transactions on Image Processing*, 2000, 9(11): 1897–1913.
11. T Y Ji, Z Lu, Q H Wu. Detection of power disturbances using morphological gradient wavelet. *Signal Processing*, 2008, 88: 255–267.
12. B Li, P L Zhang, S S Mi, et al. An adaptive morphological gradient lifting wavelet for detecting bearing faults. *Mechanical Systems and Signal Processing*, 2012, 29: 415–427.
13. J F Zhang, J S Smith, Q H Wu. Morphological undecimated wavelet decomposition for fault location on power transmission lines. *IEEE Transactions on Circuits and systems*, 2006, 53(6): 1395–1402.
14. R J Hao, F L Chu. Morphological undecimated wavelet decomposition for fault diagnostics of rolling element bearings. *Journal of Sound and Vibration*, 2009, 320(4–5): 1164–1177.
15. Y Zhang, T Y Ji, M S Li, et al. Identification of power disturbances using generalized morphological open-closing and close-opening undecimated wavelet. *IEEE Transactions on Industrial Electronics*, 2016, 63(4): 2330–2339.
16. C Li, M Liang, Y Zhang, et al. Multi-scale autocorrelation via morphological wavelet slices for rolling element bearing fault diagnosis. *Mechanical Systems and Signal Processing*, 2012, 31: 428–446.
17. G Piella, H Heijmans. Adaptive lifting schemes with perfect reconstruction. *IEEE Transactions on Signal Processing*, 2002, 50(7): 1620–1630.
18. L Bo, C Peng, X F Liu. A novel redundant haar lifting wavelet analysis based fault detection and location technique for telephone transmission lines. *Measurement*, 2014, 51: 42–52.
19. Z Lu, J S Smith, Q H Wu. Morphological lifting scheme for current transformer saturation detection and compensation. *IEEE Transactions on Circuits and Systems*, 2008, 55(10): 3349–3357.
20. Y F Li, X H Liang, M J Zuo. Diagonal slice spectrum assisted multi-scale morphological filter for rolling element bearing fault diagnosis. *Mechanical Systems and Signal Processing*, 2017, 85: 146–161.
21. Y F Li, M J Zuo, J H Lin, et al. Fault detection method for railway wheel flat using an adaptive multiscale morphological filter. *Mechanical Systems and Signal Processing*, 2017, 84: 642–658.
22. I S Bozchalooi, M Liang. A smoothness index-guided approach to wavelet parameter selection in signal de-noising and fault detection. *Journal of Sound and Vibration*, 2007, 308(1–2): 246–267.
23. N G Nikolaou, I A Antoniadis. Demodulation of vibration signals generated by defects in rolling element bearings using complex shifted Morlet waves. *Mechanical Systems and Signal Processing*, 2002, 16(4): 677–694.
24. K C Gryllias, I Antoniadis. A peak energy criterion (P.E.) for the selection of resonance bands in complex shifted Morlet wavelet (CSMW) based demodulation of defective rolling element bearing vibration response. *International Journal of Wavelets Multiresolution and Information Processing*, 2009, 7(4): 387–410.
25. C Li, M Liang, T Y Wang. Criterion fusion for spectral segmentation and its application to optimal demodulation of bearing vibration signals. *Mechanical Systems and Signal Processing*, 2015, 64–65: 132–148.
26. R B Randall, J Antoni, S Chobsaard. The relationship between spectral correlation and envelope analysis in the diagnostics of bearing faults and other cyclostationary machine signals. *Mechanical Systems and Signal Processing*, 2001, 15(5): 945–962.
27. C Li, M Liang. Continuous-scale mathematical morphology-based optimal scale band demodulation of impulsive feature for bearing defect diagnosis. *Journal of Sound and Vibration*, 2012, 331(26): 5864–5879.

Yi-Fan Li born in 1985, is a postdoctor at *School of Mechatronics Engineering, University of Electronic Science and Technology of China*. He received his PhD degree from *Southwest Jiaotong University, China*, in 2013. His main research interests include mechanical fault detection and diagnosis. E-mail: liyifan@home.swjtu.edu.cn.

MingJian Zuo Professor in Mechanical Engineering, is affiliated with the *University of Electronic Science and Technology of China* and the *University of Alberta, Canada*. His research interests include reliability analysis, maintenance optimization, diagnostics, and prognostics. E-mail: Ming.Zuo@UAlberta.CA.

Ke Feng born in 1992, is currently a PhD candidate at *Tribology and Machine Condition Monitoring Laboratory, University of New South Wales, Australia*. He received his master degree from *University of Electronic Science and Technology of China*, in 2017. His research interests include machine condition monitoring. E-mail: Wenke_Feng@126.com.

Yue-Jian Chen born in 1991, is a PhD candidate majoring in Mechanical Engineering at the *University of Alberta, Canada*. He received his Master of Science degree from *Nanjing University of Science and Technology, China*, in 2015. His main research interests include signal processing, condition monitoring, and fault diagnosis. E-mail: yuejian1@ualberta.ca.